ELSEVIER

Journal of Molecular Graphics and Modelling 20 (2001) 169–182

Journal of Molecular Graphics and Modelling

www.elsevier.com/locate/JMGM

Flexibility of the murine prion protein and its Asp178Asn mutant investigated by molecular dynamics simulations

Jörg Gsponer, Philippe Ferrara, Amedeo Caflisch*

Department of Biochemistry, University of Zürich, Winterthurerstrasse 190, CH-8057 Zürich, Switzerland

Received 8 March 2001; received in revised form 21 June 2001; accepted 28 June 2001

Abstract

Inherited forms of transmissible spongiform encephalopathy, e.g. familial Creutzfeldt–Jakob disease, Gerstmann–Sträussler–Scheinker syndrome and fatal familial insomnia, segregate with specific point mutations of the prion protein. It has been proposed that the pathologically relevant Asp178Asn (D178N) mutation might destabilize the structure of the prion protein because of the loss of the Arg164–Asp178 salt bridge. Molecular dynamics simulations of the structured C-terminal domain of the murine prion protein and the D178N mutant were performed to investigate this hypothesis. The D178N mutant did not deviate from the NMR conformation more than the wild type on the nanosecond time scale of the simulations. In agreement with CD spectroscopy experiments, no major structural rearrangement could be observed for the D178N mutant, apart from the N-terminal elongation of helix 2. The region of structure around the disulfide bridge deviated the least from the NMR conformation and showed the smallest fluctuations in all simulations in agreement with hydrogen exchange data of the wild type prion protein. Large deviations and flexibility were observed in the segments which are ill-defined in the NMR conformation. Moreover, helix 1 showed an increased degree of mobility, especially at its N-terminal region. The dynamic behavior of the D178N mutant and its minor deviation from the folded conformation suggest that the salt bridge between Arg164 and Asp178 might not be crucial for the stability of the prion protein.

Keywords: MD simulations; Prion; Multiple simulations; D178N mutant; Structural rearrangement

1. Introduction

An increasing body of experimental evidence indicates that prions are the cause of transmissible spongiform encephalopathies (TSEs) [1–4]. TSEs include kuru, Creutzfeldt–Jakob disease, fatal familial insomnia and Gerstmann–Sträussler–Scheinker syndrome in humans, scrapie in sheep, and bovine spongiform encephalopathy [5–7]. Such prion diseases can appear sporadically or as infectious or inherited disorders [8], characterized by the accumulation of an abnormal isoform (PrP^{Sc}) of the cellular prion protein (PrP^{C}) in the brain [9,10]. According to the "protein only" hypothesis [11–13], the infectious agent of TSE has no nucleic acid and is composed mostly, if not entirely, of PrP^{Sc}. This disease-associated form is identical in its covalent structure to PrP^{C} [14], and the two forms seem only to differ in their three-dimensional structure. Fourier-transform infrared and circular dichroism (CD) spectra indicate that PrP^{Sc} has an increased content of β-sheet conformation compared to PrP^{C} [15,16].

Mammalian PrP^{C} is a highly conserved secretory cell surface glycoprotein of 209 residues (208 residues in murine PrP^{C} ($mPrP^{C}$)) [17,18]. It is anchored to the cell membrane via a glycosyl phosphatidylinositol (GPI) anchor at the C-terminus and has a single disulfide bridge (Cys179–Cys214) and two *N*-glycosylation sites [14]. The nuclear magnetic resonance (NMR) solution structure of the recombinant $mPrP^{C}$ (23–231) reveals that the N-terminal segment 23–120 is disordered, while the C-terminal segment 121–231 forms a structured domain [19–21]. The three-dimensional structure of this domain is shown in Fig. 1. It consists of a small two-stranded anti-parallel β-sheet and three α-helices. The flexible loop 167–171, the last two turns of helix 2 (188–193), and the residues 220–226, containing the helix-like segment 222–226, are structurally disordered [20]. Recently, Zahn et al. have determined the NMR solution structure of the recombinant human PrP^{C}, $hPrP^{C}$ (23–231) [22]. The conformation of the $mPrP^{C}$ differs only slightly from that of the $hPrP^{C}$. In $mPrP^{C}$, helix 3 ends at residue 219, followed by a kink and the helix-like segment 222–226. The $hPrP^{C}$ has a longer helix 3 which comprises the residues 200–228.

The structured domain of PrP^{C} can adopt alternative, non-native conformations depending on the solution

* Corresponding author. Tel.: +41-1-635-55-21; fax: +41-1-635-57-12.
E-mail address: caflisch@bioc.unizh.ch (A. Caflisch).

1093-3263/01/$ – see front matter
PII: S1093-3263(01)00117-6

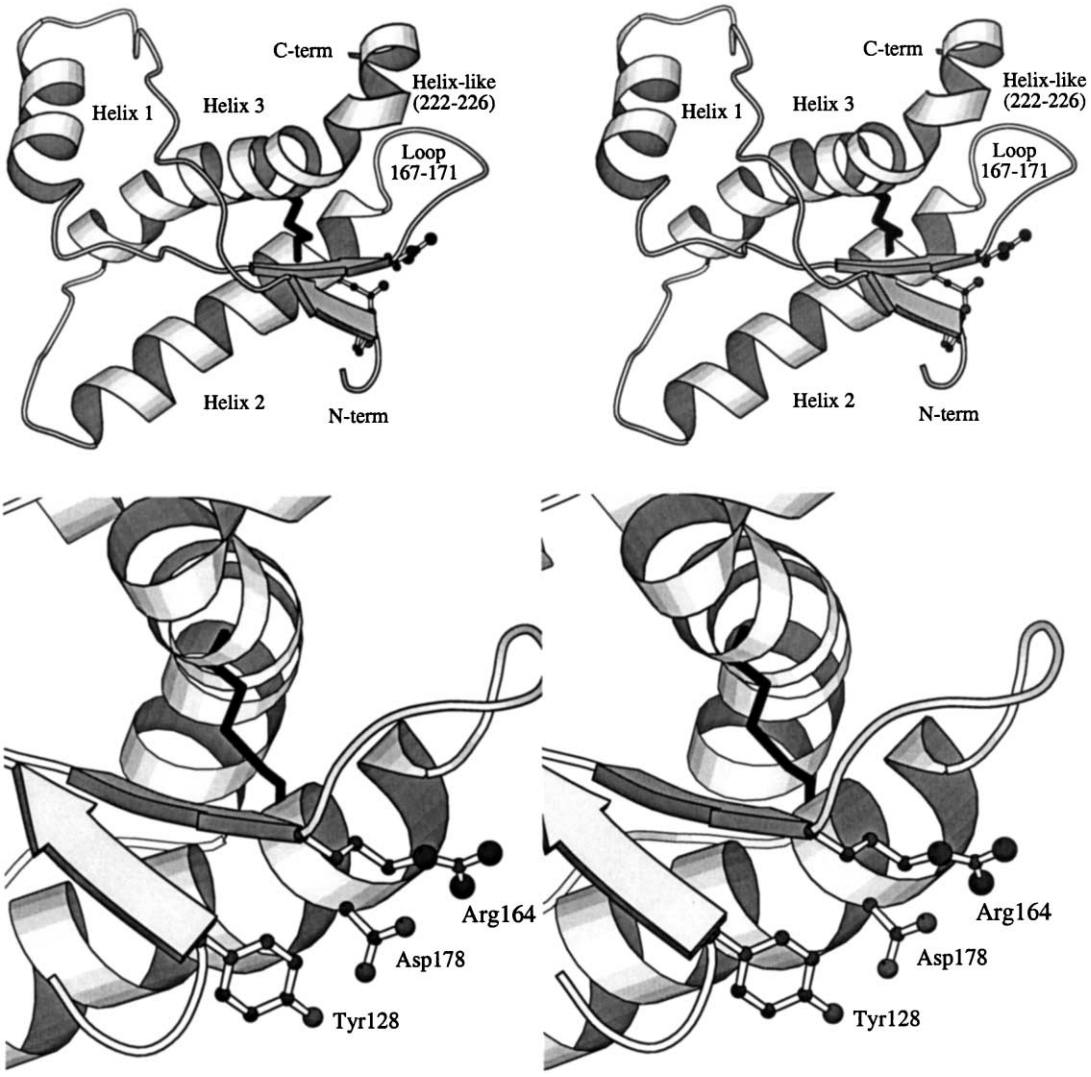

Fig. 1. (Top) Stereoview of the refined NMR solution structure of the murine PrP (124–226). The disordered chain-terminal segments 121–123 and 227–231 are ill-defined, and therefore, not shown. The disulfide bridge between Cys179 and Cys214 is identified by black bonds. Secondary structure elements are defined according to the NMR data [20]. (Bottom) Stereoview of the region close to the side chains of Tyr128, Arg164 and Asp178. Asp178 is replaced by Asn in the mutant simulations. The orientation is rotated by about 50° with respect to the stereoview in the top. The image was prepared using MOLSCRIPT [68].

conditions [23–25]. An increase of β-sheet content could be observed at low pH values [24,25] or at pH 5 and 328 K [23]. Therefore, it has been suggested that PrP^C has a high conformational plasticity, which permits it to be in dynamic equilibrium with alternative conformations [23,26]. Since the structured domain of PrP^C holds 8 of 12 specific point mutations linked with familial TSE forms [27,28], it has been proposed that the thermodynamic stability of PrP^C decreases upon mutation, and thus, further facilitates its conversion into alternative conformations like PrP^{Sc} [26,29].

Molecular dynamics (MD) simulations have become a powerful tool for studying the structure and dynamics of biomolecules. The reversible folding of miniprotein motifs has been simulated with an implicit model of the solvent [30–32]. However, MD studies with full atomic representation of the protein and solvent are usually limited to few nanoseconds. Therefore, even for small proteins they are not long enough to describe the inter-conversion between native and non-native states at room temperature. Nevertheless, MD simulations started from the X-ray or NMR conformation can provide information concerning the flexibility and the contribution of backbone and side chain interactions to local structural rearrangements of the folded state [33,34]. The flexibility of a structure is reflected in the fluctuations of each atom relative to its average position during the trajectory. Useful insights can be obtained by comparing the mobility of similar proteins or the same protein under different pH [35,36] or temperature conditions [33]. Recently, the effect of low pH on the wild type Syrian hamster PrP^C (109–219) conformation was investigated by two 10 ns MD simulations at neutral and low pH [37]. At low pH, a larger flexibility was observed throughout the

sequence and the native β-sheet structure increased. It was proposed that the neutralization of Asp178 at low pH removes interactions that inhibit a structural change at neutral pH. MD simulations have also been performed to investigated the dynamical and structural behavior of a homology model of the $hPrP^C$ (90–230) and the Syrian hamster PrP^C (90–231) [38] as well as the $mPrP^C$ (121–231) [39]. The simulations by Zuegg and Gready indicate that electrostatic interactions play an important role in the dynamic stability of PrP^C and that a correct treatment of the long-range electrostatic interactions is necessary to obtain stable trajectories [38]. To investigate the influence of the glycosylation and the GPI anchor on the structural and dynamical behavior of PrP^C, Zuegg and Gready also performed MD simulations of the homology model of $hPrP^C$ (90–230) with the two N-linked glycans (at Asn181 and Asn197) and the GPI anchor attached to Ser230 [40]. The results suggest that the N-linked glycans reduce the flexibility in some parts of the $hPrP^C$ (helices 2 and 3) and increase it in others (flexible loop 167–171). However, the *N*-glycans had no major influence on the overall conformational properties of $hPrP^C$. The importance of N-linked glycosylation was also investigated by short (100 ps) MD runs of the $mPrP^C$ and mutants thereof with or without glycan in vacuo with a distance dependent screening function [41]. Short MD simulations (500 ps) have been also performed using a small layer of explicit water molecules [42].

In this paper, the dynamical behavior of the structured domain of the wild type PrP^C and the Asp178Asn mutant is studied by explicit water MD simulations. Three runs of the wild type PrP^C and two of the Asp178Asn mutant (D178N) were performed for a total simulation time of 7.5 ns. The minimized average NMR solution conformation of $mPrP^C$ (124–226) was used as initial conformation because the $hPrP^C$ structure was not available when the simulations were started. The segment 124–226 is of pathological interest, since it has been suggested that helix 1 (144–154) might be involved in the conformational change leading from PrP^C to PrP^{Sc} [2,43]. Moreover, structural rearrangements of the D178N mutant are expected in this segment [44]. Two different phenotypes of the prion disease segregate with the replacement of Asp178 by Asn, depending on the nature of the amino acid in position 129, i.e. Met129/Asn178 correlates with fatal familial insomnia and Val129/Asn178 with Creutzfeldt–Jakob disease [45]. The simulations reported here were done with a Met in position 129. As the Asp178 side chain is involved in a salt bridge with Argl64 and a hydrogen bond with Tyr128, both connecting helix 2 with the β-sheet (Fig. 1), it was predicted that the replacement of Asp178 by Asn would lead to structural rearrangements [44]. The D178N mutant is 1.7 kcal mol^{-1} less stable than the wild type according to site-directed mutagenesis and urea-induced equilibrium transition experiments [44].

The main objective of this study was to test the hypothesis of structural rearrangements due to the D178N mutation and to investigate whether this increases the flexibility of the prion protein. In addition, the comparison of the simulation results with hydrogen exchange data [46] is useful to validate the former and extrapolate on the initial events responsible for the PrP^C to PrP^{Sc} conversion. In the MD simulations, no major displacements could be observed in the β-sheet and helix 2. Four structural elements remained close to the NMR structure in all simulations; these are the C-terminal part of helix 1, most of helices 2 and 3, and the second β-strand. Larger deviations and a higher flexibility were observed in regions which are ill-defined in the NMR structure, as well as at the N-terminal part of helix 1.

2. Methods

2.1. Simulation method

The CHARMM program [47] with the all-hydrogen CHARMM22 parameter set [48] was used for all simulations. The modified TIP3P model was employed for the water molecules [49,50]. As the NMR structure of $mPrP^C$ (protein data bank (PDB) code 1AG2) does not contain the coordinates of the ill-defined first three and last five residues of the domain 121–231, simulations were done with the segment 124–226. For the D178N mutation, one oxygen of the carboxyl group was replaced by a NH_2. The NMR structure of $mPrP^C$ (124–226) and the D178N mutant were minimized by 400 steps of steepest descent and 600 steps of conjugate gradient to relieve local strain. The minimized conformations were then immersed in an equilibrated water sphere of 36 Å radius. Water molecules overlapping the protein atoms were deleted. The criterion for overlapping was a distance smaller than 2.8 Å between the water oxygen and any heavy atom of the protein. The solvent was equilibrated for 1 ps around the rigid protein. The same sphere was overlaid four times with different orientations to fill holes in the water structure. After each overlay, all water within 2.8 Å from any protein heavy atom or other water molecule were deleted [51], and the solvent equilibrated for 1 ps. The final molecular system consisted of the prion protein (1675 and 1677 atoms for the wild type and D178N mutant, respectively) centered in a sphere of 36 Å radius with 6212 (wild type) and 6216 (D178N) water molecules. Atoms in the spherical region of 32 Å radius were treated by Newtonian dynamics, whereas the water molecules in the spherical shell from 32 to 36 Å were treated by Langevin dynamics. A deformable spherical boundary potential [52] was used to minimize the boundary effects. It has been shown that spherical boundary conditions do not affect the dynamics more than periodic boundary conditions [53]. The MMFP option of the CHARMM program was used to constrain the protein on the center of the water sphere by imposing a harmonic potential on the protein's center of mass [54]. The length of covalent bonds involving hydrogen atoms were constrained using the SHAKE algorithm [55] and the leap-frog integrator was

used with an integration step of 2 fs. The non-bonding pair list was updated every 20 steps. The CHARMM22 default cutoffs for long-range interactions were used, i.e. a shift function was used for the electrostatic term with a cutoff at 12 Å, and a switch truncation acting between 10 and 12 Å was employed for the van der Waals interactions [48]. Structures were saved every 0.5 ps for a total of 3000 snapshots for each trajectory. During an initial heating phase of 60 ps, the velocities were scaled to the final temperature of 300 K. Three simulations of the wild type (WT1–3) and two of the mutant (D178N1 and 2) were performed with different seeds for the random number generator used for the assignment of the velocities. Each simulation required approximately 2 months of CPU time on a 195 MHz R10000 processor.

2.2. Analysis methods

For the calculation of the root mean square (RMS) fluctuations relative to the average structure, the coordinate frames from the trajectories were first superimposed on the NMR conformation to remove any effect of overall translation and rotation. The RMS fluctuations are given by

$$\text{RMS fluctuations} = \langle d^2_{\text{traj, avg}} \rangle^{1/2} \quad (1)$$

where $d_{\text{traj,avg}}$ is the distance between the actual coordinates and the average position over the selected time interval, and $\langle\,\rangle$ represents the time average.

The hydrogen bond criterion consisted of a distance between the amide hydrogen and the oxygen smaller than 2.6 Å and the angle N–H$\cdots$O larger than 120°. A salt bridge was considered to be present if the distance between the donor and acceptor atoms was smaller than the sum of the van der Waals radii plus 1.5 Å [38]. Analysis of the secondary structure content was done with the program DSSP [56]. DSSP classifies the structural features of a residue according to its hydrogen bonding patterns. An *n*-turn is identified by a hydrogen bond between the CO group of residue *i* and the NH group of residue $i + n$. At least two consecutive hydrogen bonds are required for an helix assignment. In this context, repeating 3-, 4-, and 5-turns are 3_{10}- , α- and π-helix, respectively. If the hydrogen bonding patterns of some residues in a given conformation are compatible with different types of helices, α-helices take precedent over π-helices, and π-helices are preferred to 3_{10}-helices. The *n*-turns which are not part of a helix are considered as hydrogen bonded turns.

3. Results

3.1. Overall behavior

In two of the three WT runs (WT2 and WT3) the C_α RMS deviation from the minimized average NMR conformation reached a plateau after 0.5 ns with an average value over the final nanosecond of 2.2 ± 0.1 and 2.2 ± 0.2 Å, respectively

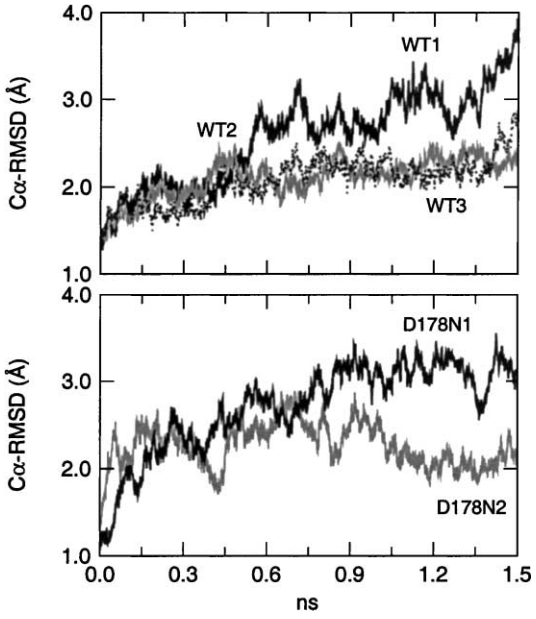

Fig. 2. Temporal evolution of the C_α RMS deviation from the minimized average NMR structure in the WT runs (upper panel) and the D178N runs (lower panel).

(Fig. 2). The C_α RMS deviation of WT1 remained at about 2.8 Å from 0.5 to 1.2 ns, but increased in the last 0.2 ns to a value of 3.7 Å. For the mutant, at the beginning of both D178N runs, the C_α RMS deviation from the minimized average NMR conformation increased faster than in the wild type simulations and reached a value of 2.5 Å already after 0.25 ns. However, in the D178N2 run, it stayed close to this value over most of the simulation time, and in the last 0.25 ns, the average C_α RMS deviation was 2.1 ± 0.1 Å. In the D178N1 run, the C_α RMS deviation increased further with an average value of 3.1 ± 0.2 Å during the final 0.5 ns.

Since there can be significant conformational heterogeneity in the NMR structures, it is useful to consider all of the NMR conformers as reference state for RMS deviation calculations. At the end of the WT1 run, the C_α RMS deviation from 11 of 20 NMR conformers is smaller than 3.0 Å (Fig. 3). In the WT2 run, the C_α RMS deviation from the 20 NMR conformers decreased with time and is smaller than 2.5 Å at 1.5 ns. Only for the conformers 9, 14 and 17 peak deviations between 3.0 and 3.5 Å were observed. WT2 remained the closest to the NMR conformer 11 with a time averaged C_α RMS deviation of 2.1 ± 0.2 Å. It is clear from Fig. 3b that there can be significant differences in the value of the RMS deviation using different NMR conformers as reference structure. The magnitude of the deviations of the WT3 run (data not shown) is in between the ones of WT1 and WT2. As for the C_α RMS deviation from the minimized average NMR structure, the deviation from the 20 NMR conformers increased in the first and showed a plateau phase in the second half of the D178N1 run. From 13 conformers, the average C_α RMS deviation was lower than 2.5 Å.

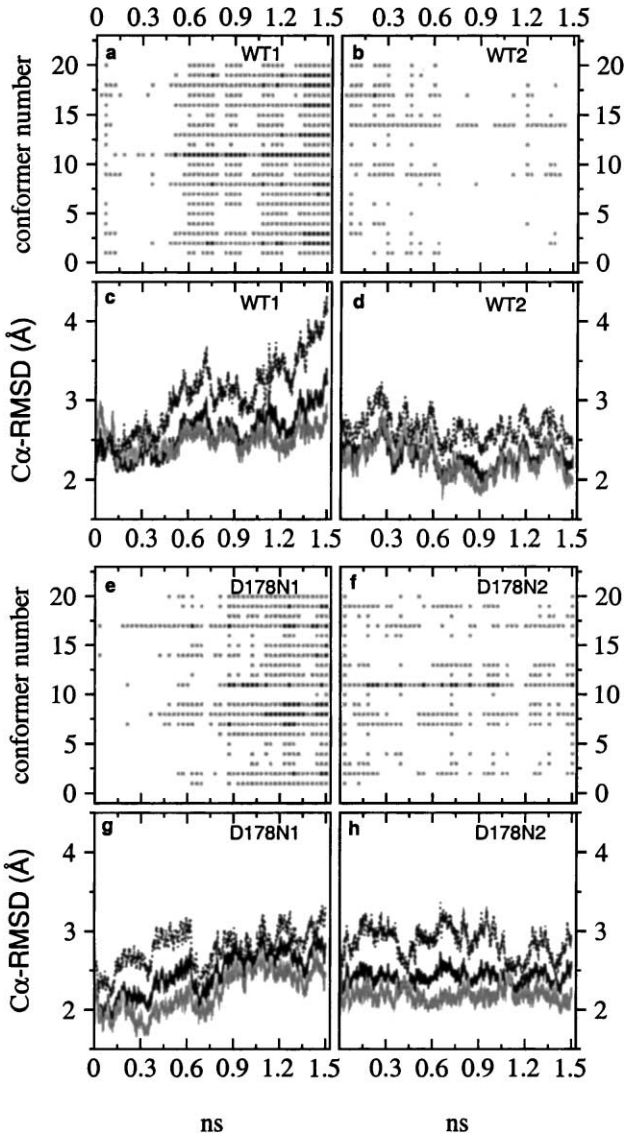

Fig. 3. ((a), (b), (e) and (f)) C_α RMS deviation from the 20 NMR conformers as a function of time. Color code: white, 0.0–2.5 Å; gray, 2.5–3.0 Å; black, >3.0 Å. ((c), (d), (g) and (h)) Evolution of the C_α RMS deviation as a function of time. The reference conformation is the NMR conformer with the smallest (gray lines) and largest (dotted lines) deviation from the final snapshot. The average value of the C_α RMS deviation from the 20 NMR conformers is shown by the black solid line.

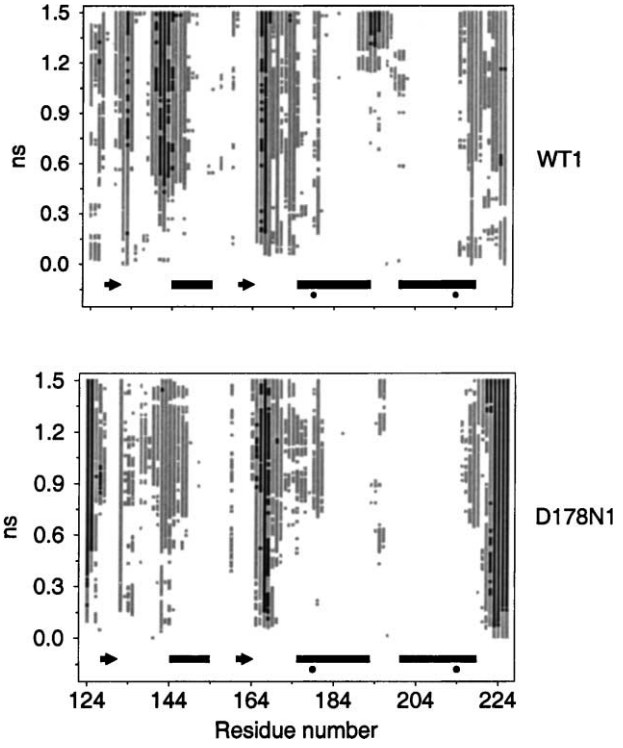

Fig. 4. C_α RMS deviation from the minimized average NMR structure as a function of residue number and time in WT1 (upper panel) and D178N1 (lower panel). Color code: white, 0.0–3.0 Å; gray, 3.0–6.0 Å; black, >6.0 Å. The secondary structure elements of $mPrP^C$ are shown at the bottom of the panels [20]. α-Helices are represented by rectangles and β-strands by arrows. The filled circles mark the position of the two cysteines forming the single disulfide bridge of the prion protein.

However, peak deviations up to 3.5 Å are seen for 11 of the 20 NMR conformers. In the D178N2 run, the C_α RMS deviation from most NMR conformers remained constant during the 1.5 ns simulation time. The average deviation from 15 of them is smaller than 2.5 Å and the lowest average value is observed for the conformer 14 with 2.2 ± 0.1 Å. Only from conformers 11, 13 and 19, the D178N2 deviated transiently >3.0 Å. Overall, this analysis indicates that the D178N simulations deviate from the NMR ensemble more than WT2 and less than WT1.

To identify the parts of the protein that underwent large displacements, it is useful to plot C_α RMS deviations as a function of residue number and time. This is shown in Fig. 4 for WT1 and D178N1, which, among the five simulations, present the largest deviations from the NMR conformers. Overall, the WT1 and D178N1 simulations show a similar behavior along the sequence and this is also true for WT2, WT3 and D178N2 (see below). In the WT1 simulation, major displacements took place in the disordered segments of the NMR solution structure, i.e. at the loop 167–171 and the C-terminus, and also in the well-defined first β-strand and the first turn of helix 1. The flexible loop 167–171 moved towards the N-terminus (Fig. 5). The deviations of the first β-strand were caused by small displacements without affecting the integrity of the two-stranded β-sheet. The first turn of helix 1 remained close to the NMR structure during the first 0.5 ns. Shortly after, it underwent an almost rigid body motion that resulted in a displacement of the the N-terminal part of helix 1 away from helix 3 (Fig. 5). This caused large deviations from the average NMR conformation mainly in the first turn of helix 1 and the final part of the segment connecting the first β-strand with helix 1 (138–143). The deviations of the first β-strand and helix 1 may be related to the fact that the former does not contribute to the hydrophobic core and the latter has only one side chain (Tyr150) in the core. Furthermore, the helix 1 residues are not involved

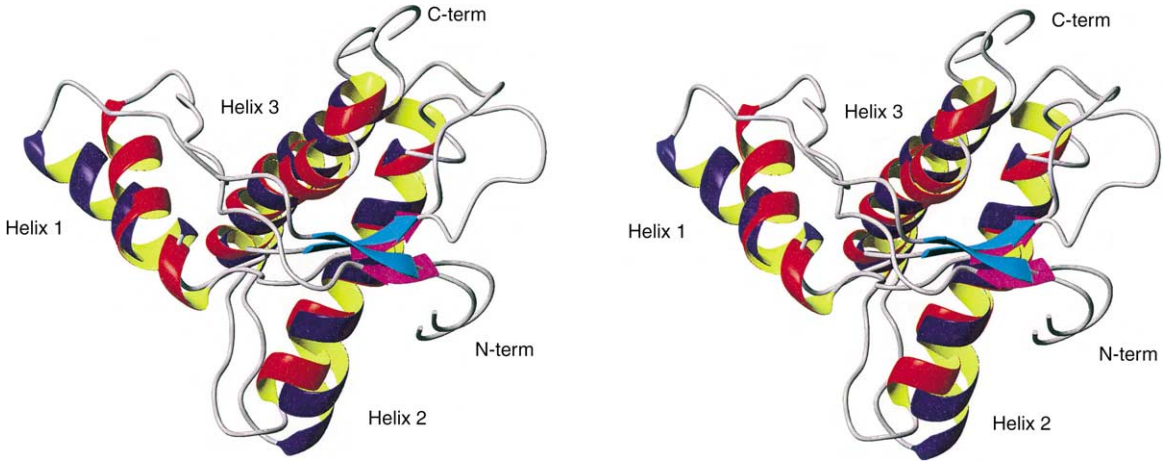

Fig. 5. Stereoview of the initial (helices in red and β-strands in magenta) and final (helices in blue and β-strands in cyan) conformation of the WT1 simulation. The picture was generated with MOLMOL [69].

in hydrogen bonds with the rest of the prion protein, except for Tyr149 and Tyr150, whose side chain hydroxyls donate to the carboxyl groups of Asp202 and the CO of Pro137 (Table 2 of [20]). The last turn of helix 2 (189–193), which belongs to an ill-defined segment in the NMR structure, showed significant deviations in the second part of the WT1 simulation due to an helical kink. This is reflected in an increasing C_α RMS deviation not only of the last turn, but also of the segment connecting helices 2 with 3 (193–199). In WT2 and WT3 (data not shown), the deviations were less pronounced, but affected the same segments as in WT1. The flexible loop 167–171 moved towards the N-terminus and the N-terminal part of helix 1 underwent an almost rigid body motion away from (WT2), respectively towards (WT3) helix 3. The amplitude of the motion of helix 1 was smaller than in WT1. Deviations higher than 3.0 Å were also seen for the segment connecting helix 2 with helix 3. However, there was no kink in helix 2 in the WT2 and WT3 runs.

In the D178N1 and D178N2 simulations, the nature and amplitude of the deviations were similar to WT1 for the loop 167–171, the C-terminus and the region of the first β-strand (Fig. 4). A displacement of the N-terminal part of helix 1 away from helix 3 could be observed in both, but it was less pronounced than in WT1 (Figs. 4 and 6). Moreover, a kink in helix 2 was transiently observed in the first part of the D178N2 simulation and disappeared at the end.

3.2. Flexibility along the sequence

The deviations described above indicate how far the protein has moved from the ensemble of NMR conformers. The C_α RMS fluctuations with respect to the average MD

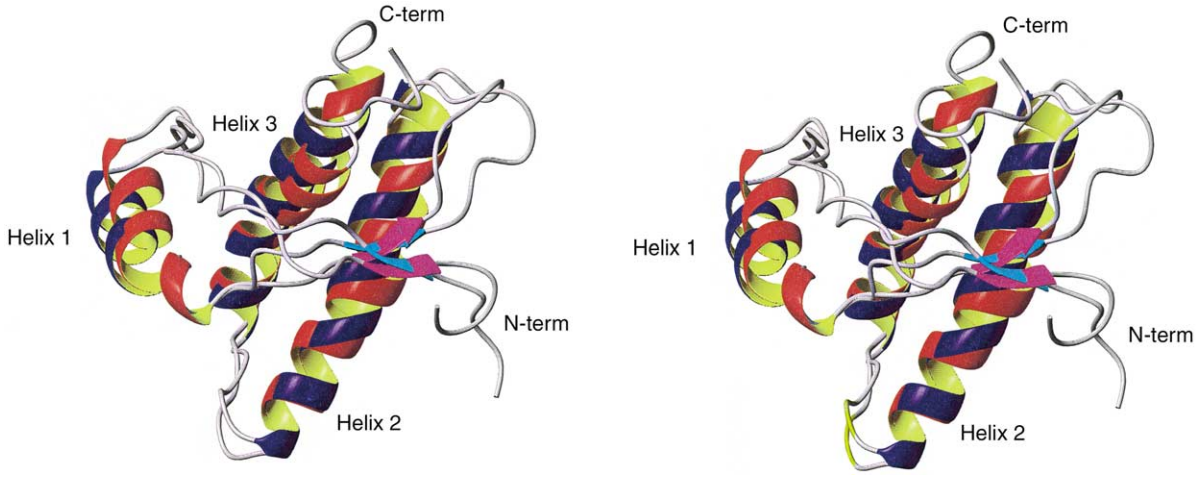

Fig. 6. Same as in Fig. 5 for the initial (helices in red and β-strands in magenta) and final (helices in blue and β-strands in cyan) conformation of the D178N1 simulation.

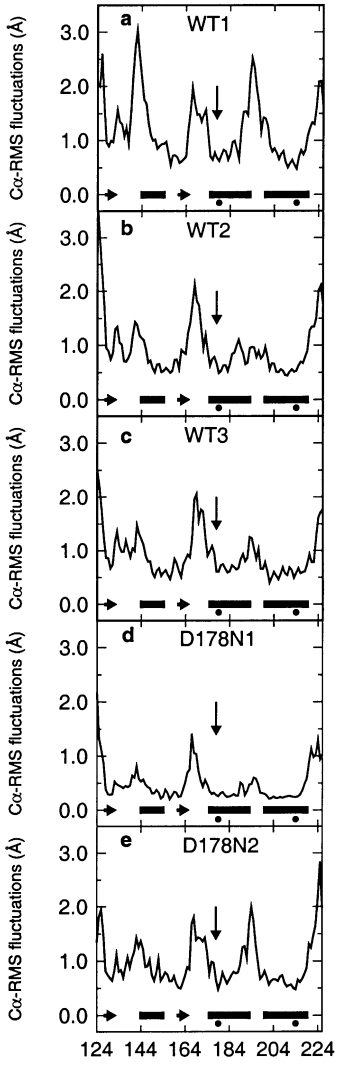

Fig. 7. C_α RMS fluctuations from the average structure of the 0.0–1.5 ns time interval as a function of residue number. The secondary structure elements and cysteine residues are represented as in Fig. 4. The arrow indicates the position of the mutation.

conformation (Fig. 7) are more appropriate to describe flexibility differences among residues. Over the whole simulation period of 1.5 ns, comparable fluctuations were found for the wild type and the D178N mutant. The residues with the smallest fluctuations are in the helices 2 and 3. They are centered around the stabilizing Cys179–Cys214 disulfide bridge (residues 178–184 and 203–218). Further, the segment 156–164, which contains the second, β-strand and contributes to the hydrophobic core with the Pro158 and Val161 side chains, shows restricted mobility. The smallest fluctuations from the averaged MD conformation were observed for the following residues: Tyr157 and the segment 210–213 in the three WT runs, and Val161 and the segment 210–214 in both D178N runs. Large fluctuations were found in the ill-defined loop 167–171, as well as at the C- and N-terminus. The flexibility of the first turn of helix 1 and the preceding segment (138–143) as well as the last turn of helix 2 and the following residues in the segment 193–199 were high in all runs, but particularly in WT1 and D178N2. This is related to their temporary large deviations from the NMR conformers. Overall, the plots in Fig. 7 indicate that the fluctuations in WT2 and WT3 are more similar to the ones of the D178N runs than to WT1. This shows that it is important to run multiple simulations and compare them. More important, it suggests that the wild type prion protein and D178N mutant show similar flexibility.

3.3. Secondary and tertiary structure stability

3.3.1. Backbone hydrogen bonds and secondary structure

Since a major shift in secondary structure content from α-helix to β-sheet is at the basis of PrP misfolding and aggregation, it is important to investigate the behavior of the main chain hydrogen bonds along the simulations. Further, the overall stability of the native configuration depends in part on the presence of backbone hydrogen bonds. Table 1 lists the occurrences of backbone hydrogen bonds during the MD simulations and compares them to the energy-minimized average NMR structure [20]. Most of the backbone hydrogen bonds of the NMR structure were present in wild type and mutant runs. However, reduced occurrences of hydrogen bonds were observed in the ill-defined fourth turn of helix 2 and the C-terminal segment 222–226. The loss of the hydrogen bonds in the fourth turn of helix 2 promoted the kink of the last turn and tended to split helix 2 in WT1 and D178N2 (Figs. 8 and 9). However, the DSSP results show that the three residues involved in the kink (Gln186, His187 and Thr188) lost the α-helical conformation only for about 10% of the WT1 and 30% of the D178N2 simulations time (Fig. 9) Further, two backbone hydrogen bonds were partially lost in structurally well-defined parts of PrP^C. They are $Arg208H^N$–Lys204O′ and $Glu152H^N$–Arg148O′. Nevertheless, the loss of these hydrogen bonds was only temporary and did not influence the continuity of the helices 1 and 3 in any run (Fig. 9). Three of the four β-sheet hydrogen bonds were present for >93% of the simulation time (Table 1). The fourth one ($Val161H^N$–Gly131O′) was present only in WT1 and D178N2. A hydrogen bond between the NH of Met134 and the CO of Asn159, which would be compatible with an elongation of the β-sheet towards the first helix, was observed only in the D178N1 simulation and for about one-half of the simulation time. Overall, the position and amount of the secondary structure elements were well preserved in the five runs (Table 2). The β-strands have a similar length in all simulations, which is slightly shorter than in the averaged NMR structure of the $mPrP^C$, but corresponds to the extent found in the NMR structure of the Syrian hamster PrP^C [57]. The length of helix 1 is the same in the five runs and just one residue shorter at the C-terminus region than in the averaged NMR conformation, whereas the helices 2 and 3 differ more. While in WT1 and WT2 their length is similar to one of the NMR solution structure, the N-terminal part

Table 1
Backbone hydrogen bonds[a]

Residue numbers[b]		Hydrogen bonds						Secondary structure[c]
HN	CO	NMR[d]	WT1[e]	WT2	WT3	D178N1	D178N2	
M129	Y163	x	100	98	96	100	100	β
G131	V161	x	100	93	99	100	100	β
M134	N159	x	**0**	**0**	**0**	51	**0**	
D147	N143		80	79	75	83	81	α1
R148	D144	x	99	97	99	97	99	α1
Y149	W145	x	91	92	86	83	87	α1
Y150	E146	x	93	93	88	98	95	α1
R151	D147	x	96	70	91	92	87	α1
E152	R148	x	**48**	**47**	52	**43**	**21**	α1
N153	Y149	x	82	90	95	98	78	α1
M154	Y150	x	97	93	72	79	96	α1
R156	N153	x	96	95	70	91	98	
V161	G131	x	62	**0**	**18**	**0**	79	β
Y163	M129	x	98	97	99	100	98	β
S170	V166		**0**	**0**	98	**0**	**0**	
H177	N173		**12**	**10**	59	77	60	α2
D178	N174		**0**	**0**	51	**48**	82	α2
C179	F175	x	78	99	**0**	98	95	α2
V180	V176	x	96	74	**0**	99	87	α2
N181	H177	x	96	92	**28**	91	70	α2
I182	D178	x	92	93	87	89	63	α2
T183	C179	x	87	86	88	93	73	α2
I184	V180	x	93	99	94	88	99	α2
K185	N181	x	91	96	88	84	91	α2
Q186	I182	x	98	97	98	99	92	α2
H187	T183	x	61	85	88	92	52	α2
T188	I184	x	96	86	100	93	98	α2
V189	K185	x	**15**	**0**	**32**	**20**	**48**	α2
T190	Q186	x	**24**	**30**	58	62	**17**	α2
T191	H187	x	75	94	99	93	**29**	α2
T192	T188	x	83	90	96	61	74	α2
T193	V189	x	93	97	83	87	87	α2
K194	T190		69	90	86	75	62	α2
V203	T199		81	87	77	58	75	α3
K204	E200	x	86	75	90	82	89	α3
M205	T201	x	87	95	98	98	97	α3
M206	D202	x	99	100	94	100	100	α3
E207	V203	x	86	69	66	92	92	α3
R208	K204	x	**21**	**22**	**0**	**23**	60	α3
V209	M205	x	87	97	83	90	91	α3
V210	M206	x	100	100	100	100	99	α3
E211	E207	x	94	89	80	91	95	α3
Q212	R208	x	77	78	**21**	88	87	α3
M213	V209	x	83	98	96	93	98	α3
C214	V210	x	100	100	100	99	100	α3
V215	E211	x	99	93	70	98	81	α3
T216	Q212	x	99	100	73	98	94	α3
Q217	M213	x	99	98	91	97	100	α3
Y218	C214	x	97	92	77	67	94	α3
Q219	V215	x	99	99	**0**	59	90	α3
K220	T216		76	86	**0**	58	61	α3
E221	Y217		48	75	**0**	50	57	α3
S222	Y218		95	96	91	77	96	α3
Q223	Q219	x	**0**	**0**	**37**	**0**	**0**	Helix-like
A224	E221	x	**0**	**0**	**0**	**0**	**28**	Helix-like
Y225	S222	x	**0**	**0**	**47**	**0**	**0**	Helix-like
Y226	S222	x	**24**	**37**	91	**17**	**0**	Helix-like

[a] This list contains the backbone hydrogen bonds in the average NMR conformation and those with occurrences larger than 50% in either the WT or D178N simulations.

[b] The hydrogen donors are given in the first column (labeled HN) and the hydrogen acceptors in the second column (labeled CO).

[c] Secondary structure elements in which the hydrogen bond is formed.

[d] Hydrogen bonds in the minimized average NMR conformation are marked with a x [20].

[e] Percentages lower than 50% are in bold.

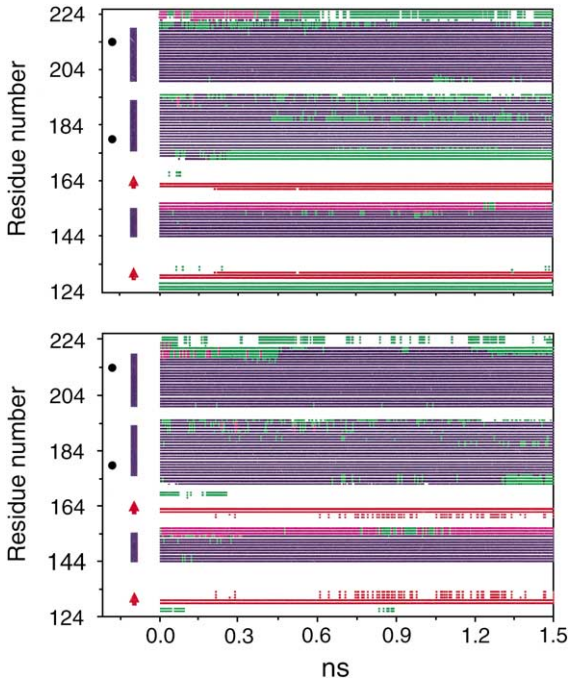

Fig. 8. Secondary structure of WT1 (upper panel) and D178N1 (lower panel) as a function of simulation time determined with DSSP [56]. The α-helix is shown in blue, the 3_{10}-helix in magenta, the H-bond turn in green and the β-strand in red. The secondary structure elements of the NMR solution structure [20] are shown on the left and are represented as in Fig. 4.

of helix 2 is shorter by 3 residues and the C-terminal part of helix 3 by one residue in WT3. The N-terminal shortening of helix 2 is associated with the formation of an additional $i - i + 4$ backbone hydrogen bond between Ser170 and Pro166 (Table 1) and the partial formation of a helical turn (Fig. 9) in the preceding flexible loop 167–171. In both mutant simulations, an N-terminal elongation of helix 2 by at least one residue was observed. This elongation is also reflected in the two backbone hydrogen bonds His177–Asn173 and Asp178–Asn174, which have a higher occurrence in the D178N than in the WT runs and may originate from the rearrangement of the region close to the mutated residue.

3.3.2. *Side chain hydrogen bonds*

The analysis of the salt bridges and side chain hydrogen bonds within helices 2 and 3 did not reveal substantial differences between the WT and D178N simulations. In helix 1, the salt bridge Asp144–Arg148 at the surface of the protein was present in all simulations. The salt bridge Asp147–Arg151, observed in >68% of all three WT simulations, was present during <25% of the D178N runs, but partially replaced by the salt bridge Glu152–Arg151. The other side chain hydrogen bonds in helix 1 behaved very similarly in WT and D178N.

Salt bridges and side chain hydrogen bonds between residues far apart in the sequence can stabilize the secondary structure [58,59]. The two most frequent charge interactions between residues distant in the sequence are Arg156–Asp202 and Arg156–Glu196 (Table 3). The former bridges the C-terminal part of helix 1 with helix 3 and the latter the C-terminal part of helix 1 with the segment between helices 2 and 3. It is interesting to note that the kink in the last turn of helix 2 was associated with the loss of the salt bridge Arg156–Glu196 in WT1 and D178N2. The D178N mutation results in the loss of the salt bridge with Arg164 and the hydrogen bond with the side chain of Tyr128 (Table 4). The disappearance of the latter was also frequently observed in the WT runs, but was water-bridged for at least 15% of the time during which the hydrogen

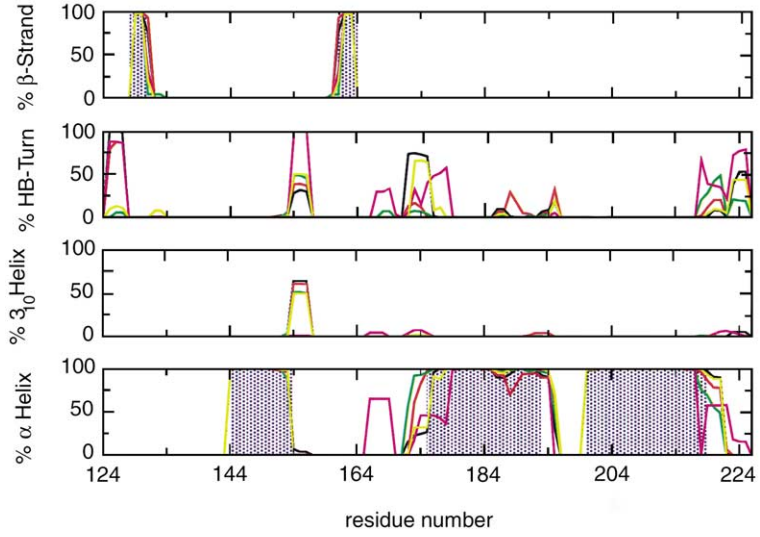

Fig. 9. Percentage of secondary structure per residue during WT1 (black), WT2 (yellow), WT3 (magenta), D178N1 (green) and D178N2 (red). The DSSP program was used to assign secondary structure [56]. The dotted regions show the extent of the β-strand (top panel) and the α-helices (bottom panel) in the NMR solution structure [20].

Table 2
Residues in regular secondary structural elements

	NMR[a]	WT1[b]	WT2	WT3	D178N1	D178N2
Helix 1	144–154	144–153	144–153	144–153	144–153	144–153
Helix 2	175–193	176–194	176–194	178–194	174–194	174–195
Helix 3	200–219	200–221	200–221	200–218	200–221	200–220
Strand β1	128–131	129–131	129–131	129–130	129–131	129–131
Strand β2	161–164	161–163	161–163	162–163	161–163	162–163

[a] Residues in regular elements of secondary structure in the minimized average NMR structure [20].
[b] Secondary structure in the WT and D178N simulations. Residue ranges were defined using DSSP [56] and averaging over the 1.5 ns time interval of each run.

Table 3
Salt bridges between residues far apart in the sequence

Salt bridges	NMR[a]	WT1[b]	WT2	WT3	D178N1	D178N2
Glu146–Lys204	**0**	**0**	**0**	**0**	**6**	**29**
Glu146–Arg208	**15**	**0**	**22**	81	**0**	**4**
Asp178–Arg164	**45**	99	**15**	88	**0**	**0**
Glu196–Arg156	80	87	100	100	100	59
Asp202–Arg156	65	98	100	100	100	100

[a] Salt bridge occurrences in the 20 NMR conformers [20]. Percentages lower than 50% are in bold.
[b] Salt bridge occurrences in the WT and D178N simulations.

Table 4
Side chain hydrogen bonds between residues far apart in the sequence

Hydrogen bonds	NMR[a]	WT1[b]	WT2	WT3	D178N1	D178N2
Tyr128H$^{\eta}$–Asx178O$^{\delta}$	**45**	**44**	**6**	**34**	**2**	**6**
Arg136H$^{\eta}$–Tyr157O	**0**	94	100	98	100	99
Arg136H$^{\epsilon}$–Pro158O	**15**	**41**	51	**5**	**13**	77
Tyr149H$^{\eta}$–Asp202O$^{\delta}$	65	**34**	100	100	100	99
Tyr150H$^{\eta}$–Pro137O	65	93	100	100	100	**23**
Tyr157H$^{\eta}$–Asp202O$^{\delta}$	**30**	71	99	94	100	92
Tyr162H$^{\eta}$–Thr183O$^{\gamma}$	**15**	98	99	61	99	97
His187H$^{\epsilon}$–Gln160O	**15**	100	100	97	100	99

[a] Hydrogen bond occurrences in the 20 NMR conformers [20]. Percentages lower than 50% are in bold.
[b] Hydrogen bond occurrences in the WT and D178N simulations.

bond was not formed. This was not the case in D178N. The salt bridge Asp178–Arg164 was broken during most of the WT2 run, without being water-bridged during its absence. The N-terminal part of helix 1 was only weakly connected to helix 3 by the new formed salt bridge Glu146–Lys204 in the D178N runs and the salt bridge Glu146–Lys208 in the WT simulations. Additionally, another non-bonding interaction between helices 1 and 3 was broken in WT1, the hydrogen bond Tyr149H$^{\eta}$–Asp202O$^{\delta}$. The rupture of this hydrogen bond was associated with the loss of hydrophobic contacts between helices 3 and 1 and the rotation of the N-terminal part of the latter away from helix 3. In all five runs, Arg136 formed a new highly occupied hydrogen bond with Tyr157, whereas the hydrogen bond with Pro158, which is present in 15% of the NMR conformers, is less frequently present. A partial loss of the hydrogen bond Tyr150H$^{\eta}$–Pro137O was seen in D178N2. However, a water molecule was inserted between Tyr150 and Pro137 for >90% of the time during which the hydrogen bond was broken. Taken together, these simulation results indicate that on the 1.5 ns time scale of the MD runs there are only minor differences in secondary structure content and charge interactions between the wild type and D178N mutant.

4. Discussion

4.1. Comparison with previous MD simulations of PrP^C

Zuegg and Gready have performed two sets of MD simulations of the PrP^C [38]. In one set of runs the non-bonding interactions were truncated at 8 Å, while in another set the long-range electrostatic interactions were included using the particle mesh Ewald (PME) approach. Stable trajectories, over a 1 ns time scale, were only obtained by treating the long-range electrostatic interactions with the PME method and by neutralizing the system with counterions. By contrast, Alonso et al., obtained a stable trajectory over 10 ns at

neutral pH by using a cutoff of 10 Å [37]. The simulations reported here were performed with a cutoff of 12 Å for the non-bonding interactions. No loss of secondary structure in the well-defined parts of the $mPrP^C$ was observed. However, the simulations indicate a wide range of dynamical behavior for this protein. In two of the three wild type runs, the conformation is stable (C_α RMS deviation smaller than 2.3 Å). In the remaining one (WT1), a deviation of 3.5 Å from the minimized average NMR conformation was observed. In the D178N mutant runs, the C_α RMS deviation from most NMR conformers remained below 3.0 Å. Taken together with the previous simulations, this shows that the variation within simulations of the same system can be larger than between different systems. This indicates that it is necessary to run multiple simulations.

All previous simulations and the ones presented in this study show a high flexibility of the loop 167–171 and the segment connecting helices 2 and 3, but different results concerning the mobility of the N-terminal part of helix 1. The analysis of the Syrian hamster PrP^C (90–231) trajectory by Parchment and Essex [39] indicates that the region between and including the first β-strand and helix 1 is rather flexible, which is not the case in their simulation of the $mPrP^C$ (121–231). They suggested that this is the consequence of the additional unstructured N-terminal region (90–120) in the Syrian hamster PrP^C. Although the simulations analyzed here were performed with the mouse sequence devoid of the unstructured N-terminal region (90–120), all WT trajectories show a high flexibility for the first turn of helix 1 and the six preceding residues (segment 138–148). This indicates that the reasons for the flexibility are complex. Moreover, a rigid body motion of the N-terminal part of helix 1 was observed in all simulations, particularly in WT1. This was not reported in the previous studies except for the low pH simulation of the Syrian hamster PrP^C (109–219) [37].

The simulations of the human and the Syrian hamster PrP^C [38] identified three highly occupied salt bridges, i.e. Glu146/Asp144–Arg208, Arg164–Asp178 and Arg156–Glu196. The latter two were also present in two of the three WT trajectories, whereas the first one showed a high occurrence only in one. In addition, the salt bridge Arg156–Asp202, connecting residues far apart in sequence, was highly occupied in the WT simulations. Zuegg and Gready suggested that electrostatic interactions, in general, and salt bridges, in particular, are important for the stability of PrP^C. It was proposed that the elimination of the salt bridge Arg164–Asp178 by mutation may loosen the structure of the prion protein [38]. The simulations reported here allow to investigate this hypothesis by a direct comparison between WT and D178N. The latter did not deviate more from the minimized average NMR conformation and the 20 NMR conformers than the WT runs. Therefore, the salt bridge Arg164–Asp178 does not seem to contribute to the overall stability of the $mPrP^C$. In WT2, which has the smallest average and final C_α RMS deviation from the average NMR conformation, the salt bridge Arg164–Asp178 was present during only 15% of the simulation time which provides further support for its negligible contribution to the dynamic stability of $mPrP^C$. Moreover, the loss of interactions in the Asp178Asn mutant might partially be compensated by N-glycosylation, as shown by experiments [60] and simulations [41].

4.2. Comparison of MD simulation results with experimental hydrogen exchange data

In the WT and D178N simulations, the C-terminal part of helix 1, most of helices 2 and 3, and the second β-strand were the most stable elements of the $mPrP^C$ structure. Recent hydrogen/deuterium exchange experiments [46] showed that the same structural elements, and in particular the residues close to the disulfide bridge have the highest protection from exchange. In contrast, the loop 167–171, the first six residues of helix 1 (144–149), the last seven residues of helix 2 (187–193), as well as the first β-strand showed no protection from exchange. These unprotected regions match with the structured parts of the PrP, which present the largest deviations from the NMR structure in the simulations. Moreover, the differences in fluctuations along the sequence seem to correlate with the hydrogen exchange results. This is in accord with the results of Bahar et al. [61], who have shown a correlation between hydrogen exchange and residue fluctuations evaluated by a simple analytical model based on local packing densities and distribution of tertiary contacts in the native state.

However, the agreement between hydrogen exchange and fluctuations in the nanosecond time scale can originate from the fact that the pattern of protection of PrP^C correlates well with the hydrophobic core structure. This is not the case for all proteins [62], although highly buried residues exchange in many cases very slowly [63]. Moreover, the high fluctuations of the N-terminal part of helix 1 reflect rigid body motions. The backbone hydrogen bonds within the first turn did not break more frequently than those in the remaining part of helix 1, which was less flexible. A similar observation was made during low temperature MD simulations of cytochrome C, which showed that large fluctuations do not necessarily correlate with hydrogen exchange [64].

4.3. Mobility of helix 1

In all simulations, high fluctuations and relatively large deviations from the NMR conformation were found in the ill-defined segments of the solution structure, namely the loop 167–171 and the C-terminus (220–226) [20]. The N-terminal part of helix 1 (residues 144–148) is also flexible and deviated more from the average NMR conformation than other structured parts of the proteins, although helix 1 is well-defined in the solution structure. Interestingly, the three flexible structural elements lie, entirely or partially, within the epitope recognized by the monoclonal antibody 15B3 [43]. This antibody can discriminate between PrP^C

and PrP^{Sc} and its epitope contains the residues 142–148, 162–170 and 214–226 [43]. The segment 142–148 is of interest, since helix 1 is set apart from the core and also away from the other epitope regions in the solution structure of PrP^{C} [19]. It has been suggested that helix 1 might be involved in the conformational change leading from PrP^{C} to PrP^{Sc} [2,43]. Recently, on the basis of CHARMM energy calculations, a theoretical model was proposed in which helix 1 rearranges in β-sheet-like manner to favor aggregation [65]. The magnitude of the rotation of the N-terminal part of helix 1 towards (WT3), and away (WT1, WT2, D178N1 and D178N2) from the core, was different in the five simulations. This motion may be explained by the almost complete lack of stabilizing tertiary contacts, neither hydrophobic nor hydrophilic, between helix 1 and the other structural elements. Overall, the analysis of helix 1 leads to the conclusion that its N-terminal region can undergo larger rigid body motions than most of the other well-defined structural elements. On the other hand, it should be pointed out that the backbone hydrogen bonds in the first turn of helix 1, as well as the three salt bridges between helix 1 residues, were stable in all simulations. Interestingly, Alonso et al. observe an approximately 10–15 Å displacement of helix 1 and the preceding loop towards helices 2 and 3 in the low pH simulation [37]. Moreover, they report a partial unfolding of helix 1.

4.4. Dynamic behavior and structural rearrangements of the D178N mutant

The hypothesis of a high conformational plasticity of PrP^{C} was used to suggest that mutations may promote the conversion of PrP^{C} into intermediate states [26,29]. The ability of mutations to increase the population of amyloidogenic folding intermediates has already been demonstrated for two naturally occurring human lysozyme variants [66]. As already mentioned in the Section 1, room temperature simulations in the nanosecond time scale do not allow to sample the inter-conversion between native and intermediate states. Nevertheless, mutations can result in different dynamic behavior of the native state and lead to partial unfolding with an increase of the RMS deviation from the NMR solution structure in a MD simulation [34].

The D178N mutation results in the loss of the hydrogen bond with the side chain of Tyr128 and salt bridge with Arg164. Yet, the final RMS deviation from the NMR solution structure is similar in the D178N and WT runs. These simulation results suggest that the interactions of Asp178 are not essential for the overall stability. This appears to be in disagreement with experimental results showing a reduced thermodynamic stability for the D178N mutant [44]. However, it has to be stressed that MD simulations with explicit water molecules give an insight on the dynamic behavior only on the nanosecond time scale and close to the native state. On the other hand, the thermodynamic stability depends on the free energy difference between the folded and the unfolded state. Therefore, even for small proteins, the time scale currently accessible by explicit water MD simulations does not allow to directly investigate thermodynamic stability, and the analysis of native state flexibility and dynamic behavior has only a qualitative significance [33,34].

The loss of the salt bridge between Arg164 and Asp178 did not lead to a decrease of secondary structure in the 1.5 ns time scale of the simulation. This is consistent with CD spectroscopy results indicating that the structural characteristics of the wild type PrP^{C} were preserved in D178N [44]. Moreover, three single-residue variants of the $hPrP^{C}$ (M166V, S170N and R220K) were shown to have the same solution conformation as the wild type bovine, human, murine and Syrian hamster PrP^{C} [67]. An elongation of the N-terminal part of helix 2 (174–175) was observed in both D178N simulations; this might be a consequence of the lack of the salt bridge. In contrast to what has been proposed based on thermodynamic stability measurements of D178N [44], no major structural rearrangements were seen between the β-sheet and helix 2. The reasons for this might be the high persistence of the backbone hydrogen bonds in the β-sheet and the hydrogen bond $Tyr162H^{\eta}$–$Thr183^{\gamma}$, which connects the second strand of the β-sheet with helix 2. The mutation Thr183Ala segregates with Creutzfeldt–Jakob disease and destabilizes $mPrP^{C}$ (121–231) by about 4.6 kcal mol^{-1} at pH 7 and 25°C [44]. It might be interesting to experimentally measure the effect of the mutations Tyr162Phe on the stability of PrP^{C}.

5. Conclusions

The MD trajectories of the D178N mutant, which is known to be a pathological variant of the $hPrP^{C}$, showed no major structural rearrangements of the protein, besides an elongation of the N-terminal part of helix 2. The dynamic behavior of D178N on the nanosecond time scale of the simulations and, in particular, its deviations from the NMR conformation, comparable to the ones of the wild type, suggest that the salt bridge between Arg164 and Asp178 might not contribute to the stability of PrP^{C}. All simulations indicate that the N-terminal region of helix 1 can undergo significant rigid body displacement. In agreement with hydrogen exchange data, the simulations results show a region with a dynamically stable behavior around the disulfide bridge, which links helices 2 and 3. Hence, helices 2 and 3 are unlikely to be among the first structured elements to unfold and adopt an alternative conformation under native state conditions.

Acknowledgements

We thank Serena Fioravanti for interesting discussions and Nicolas Budin for computer support. We also thank Dr. R. Riek for sending us the 20 NMR conformers of the murine prion protein. This work was supported by the Olga

Mayenfisch foundation and the Swiss National Science Foundation (Grant 31-53604.98 to AC). J.G. is a fellow of the M.D.–Ph.D. program of the Swiss National Science Foundation (Grant 3236-057617).

References

[1] S.B. Prusiner, Molecular biology of prion diseases, Science 252 (1991) 1515–1522.
[2] S.B. Prusiner, Prions, Proc. Natl. Acad. Sci. U.S.A. 95 (1998) 13363–13383.
[3] C. Weissmann, The ninth Datta lecture. Molecular biology of transmissible spongiform encephalopathies, FEBS Lett. 389 (1996) 3–11.
[4] M.R. Scott, R. Will, J. Ironside, H.O. Nguyen, P. Tremblay, S.J. DeArmond, S.B. Prusiner, Compelling transgenetic evidence for transmission of bovine spongiform encephalopathy prions to humans, Proc. Natl. Acad. Sci. U.S.A. 96 (1999) 15137–15142.
[5] C. Weissmann, M. Fischer, A. Raeber, H. Bueler, A. Sailer, D. Shmerling, T. Rulicke, S. Brandner, A. Aguzzi, The role of PrP in pathogenesis of experimental scrapie, Cold Spring Harb. Symp. Quant. Biol. 61 (1996) 511–522.
[6] S. Prusiner, Prion diseases and the BSE crisis, Science 278 (1997) 245–251.
[7] J.W. Ironside, Prion diseases in man, J. Pathol. 186 (1998) 227–234.
[8] F.E. Cohen, S.B. Prusiner, Pathologic conformations of prion proteins, Ann. Rev. Biochem. 67 (1998) 793–819.
[9] S. Liemann, R. Glockshuber, Transmissible spongiform encephalopathies, Biochem. Biophys. Res. Commun. 250 (1998) 187–193.
[10] R. Kordek, J.A. Hainfellner, P.P. Liberski, H. Budka, Deposition of the prion protein (PrP) during the evolution of experimental Creutzfeldt–Jakob disease, Acta Neuropathol. 98 (1999) 597–602.
[11] T. Alper, W.A. Cramp, D.A. Haig, M.C. Clarke, Does the agent of scrapie replicate without nucleic acid? Nature 214 (1967) 764–766.
[12] J.S. Griffith, Self-replication and scrapie, Nature 215 (1967) 1043–1044.
[13] S.B. Prusiner, Novel proteinaceous infectious particles cause scrapie, Science 216 (1982) 136–144.
[14] N. Stahl, S.B. Prusiner, Prions and prion proteins, FASEB J. 5 (1991) 2799–2807.
[15] B.W. Caughey, A. Doug, K.S. Bhat, D. Ernst, S.F. Hayes, W.S. Caughey, Secondary structure analysis of the scrapie-associated protein PrP 27–30 in water by infrared spectroscopy, Biochemistry 30 (1991) 7672–7680.
[16] K.M. Pan, M.A. Baldwin, J. Nguyen, M. Gasset, A. Serban, D. Groth, I. Mehlhorn, Z. Huang, R.J. Fletterick, F.E. Cohen, S.B. Prusiner, Conversion of α-helices into β-sheets features in the formation of the scrapie prion proteins, Proc. Natl. Acad. Sci. U.S.A. 90 (1993) 10962–10966.
[17] H.M. Schatzl, M. Da Costa, L. Taylor, F.E. Cohen, S.B. Prusiner, Prion protein gene variation among primates, J. Mol. Biol. 245 (1995) 362–374.
[18] M. Billeter, R. Riek, G. Wider, S. Hornemann, R. Glockshuber, K. Wüthrich, Prion protein NMR structure and species barrier for prion diseases, Proc. Natl. Acad. Sci. U.S.A. 94 (1997) 7281–7285.
[19] R. Riek, S. Hornemann, G. Wider, M. Billeter, R. Glockshuber, K. Wüthrich, NMR structure of the mouse prion protein domain PrP (121–231), Nature 382 (1996) 180–182.
[20] R. Riek, G. Wider, M. Billeter, S. Hornemann, R. Glockshuber, K. Wüthrich, Prion protein NMR structure and familial human spongiform encephalopathies, Proc. Natl. Acad. Sci. U.S.A. 95 (1998) 11667–11672.
[21] R. Riek, S. Hornemann, G. Wider, R. Glockshuber, K. Wüthrich, NMR characterization of the full-length recombinant murine prion protein, mPrP (121–231), FEBS Lett. 413 (1997) 282–288.
[22] R. Zahn, A. Liu, T. Luhrs, R. Riek, C. von Schroetter, F. Lopez Garcia, M. Billeter, L. Calzolai, G. Wider, K. Wüthrich, NMR solution structure of the human prion protein, Proc. Natl. Acad. Sci. U.S.A. 97 (2000) 145–150.
[23] H. Zhang, J. Stockel, I. Mehlhorn, D. Groth, M.A. Baldwin, S.B. Prusiner, T.L. James, F.E. Cohen, Physical studies of conformational plasticity in a recombinant prion protein, Biochemistry 36 (1997) 3543–3553.
[24] S. Hornemann, R. Glockshuber, A scrapie-like unfolding intermediate of the prion protein domain PrP (121–231) induced by acidic pH, Proc. Natl. Acad. Sci. U.S.A. 95 (1998) 6010–6014.
[25] W. Swietnicki, R. Petersen, P. Gambetti, W. Surewicz, pH-dependent stability and conformation of the recombinant human prion protein PrP (90–231), J. Biol. Chem. 272 (1997) 27517–27520.
[26] F.E. Cohen, K.M. Pan, Z. Huang, M. Baldwin, R.J. Fletterick, S.B. Prusiner, Structural clues to prion replication, Science 264 (1994) 530–531.
[27] S.B. Prusiner, Molecular biology and pathogenesis of prion diseases, Trends Biochem. Sci. 21 (1996) 482–487.
[28] L.G. Goldfarb, P. Brown, L. Cervenakova, D.C. Gajdusek, Genetic analysis of Creutzfeldt–Jakob disease and related disorders, Phil. Trans. R. Soc., Lond. B Biol. Sci. 343 (1994) 379–384.
[29] Z. Huang, J.M. Gabriel, M.A. Baldwin, R.J. Fletterick, S.B. Prusiner, F.E. Cohen, Proposed three-dimensional structure for the cellular prion protein, Proc. Natl. Acad. Sci. U.S.A. 91 (1994) 7139–7143.
[30] P. Ferrara, A. Caflisch, Folding simulations of a three-stranded anti-parallel β-sheet peptide, Proc. Natl. Acad. Sci. U.S.A. 97 (2000) 10780–10785.
[31] A. Hiltpold, P. Ferrara, J. Gsponer, A. Cafiisch, Free energy surface of the helical peptide Y(MEARA)6, J. Phys. Chem. B 104 (2000) 10080–10086.
[32] P. Ferrara, A. Caflisch, Native topology or specific interactions: what is more important for peptide folding? J. Mol. Biol. 306 (2001) 837–850.
[33] T. Lazaridis, I. Lee, M. Karplus, Dynamics and unfolding pathways of a hyperthermophilic and a mesophilic rubredoxin, Protein Sci. 6 (1997) 2589–2605.
[34] L. Wang, Y. Duan, R. Shortle, B. Imperiali, P.A. Kollman, Study of the stability and unfolding mechanism of BBA1 by molecular dynamics simulations at different temperatures, Protein Sci. 8 (1999) 1292–1304.
[35] A. Caflisch, M. Karplus, Acid and thermal denaturation of barnase investigated by molecular dynamics simulations, J. Mol. Biol. 252 (1995) 672–708.
[36] A. Caflisch, M. Karplus, Structural details of urea binding to barnase: a molecular dynamics analysis, Structure 7 (1999) 477–488.
[37] D.O. Alonso, S.J. DeArmond, F.E. Cohen, V. Daggett, Mapping the early steps in the pH-induced conformational conversion of the prion protein, Proc. Natl. Acad. Sci. U.S.A. 98 (2001) 2985–2989.
[38] J. Zuegg, J.E. Gready, Molecular dynamics simulations of human prion protein: importance of correct treatment of electrostatic interactions, Biochemistry 38 (1999) 13862–13876.
[39] O.G. Parchment, J.W. Essex, Molecular dynamics of the mouse and Syrian hamster PrP: implications for activity, Proteins: Struct. Funct. Genet. 38 (2000) 327–340.
[40] J. Zuegg, J.E. Gready, Molecular dynamics simulation of human prion protein including both N-linked oligosaccharides and the GPJ anchor, Glycobiology 10 (2000) 959–974.
[41] N.K. Wong, D.V. Renouf, S. Lehmann, E.F. Hounsell, Glycosylation of prions and its effects on protein conformation relevant to amino acid mutations, J. Mol. Graphics Modell. 18 (2000) 126–134, 163–165.
[42] M. Billeter, K. Wüthrich, The prion protein globular domain and disease-related mutants studied by molecular dynamics simulations, Arch. Virol. Suppl. (2000) 251–263.
[43] C. Korth, B. Stierli, P. Streit, M. Moser, O. Schaller, R. Fischer, W. Schulz-Schaeffer, H. Kretzschmar, A. Raeber, U. Braun, F.

Ehrensperger, S. Hornemann, R. Glockshuber, R. Riek, M. Billeter, K. Wüthrich, B. Oesch, Prion (PrP^{Sc})-specific epitope defined by a monoclonal antibody, Nature 390 (1997) 74–77.

[44] S. Liemann, R. Glockshuber, Influence of amino acid substitutions related to inherited human prion diseases on the thermodynamic stability of the cellular prion protein, Biochemistry 38 (1999) 3258–3267.

[45] L.G. Goldfarb, R.B. Petersen, M. Tabaton, P. Brown, A.C. LeBlanc, P. Montagna, P. Cortelli, J. Julien, C. Vital, W.W. Pendelbury, M. Haltia, P.R. Wills, J.J. Hauw, P.E. McKeever, L. Monari, B. Schrank, G.D. Swergold, L. Autilio-Gambetti, D.C. Gajdusek, E. Lugaresi, P. Gambetti, Fatal familial insomnia and familial Creutzfeldt–Jakob disease: disease phenotype determined by a DNA polymorphism, Science 258 (1992) 806–808.

[46] L.L. Hosszu, N.J. Baxter, G.S. Jackson, A. Power, A.R. Clarke, J.P. Waitho, C.J. Craven, J. Collinge, Structural mobility of the human prion protein probed by backbone hydrogen exchange, Nature Struct. Biol. 6 (1999) 740–743.

[47] B.P. Brooks, P.E. Bruccoleri, B.D. Olafson, D.J. States, S. Swaminathan, M. Karplus, CHARMM: a program for macromolecular energy, minimization, and dynamics calculations, J. Comput. Chem. 4 (1983) 187–217.

[48] A.D. MacKerell, D. Bashford, M. Bellott, R.L. Dunbrack, J.D. Evanseck, M.J. Field, S. Fischer, J. Gao, H. Guo, S. Ha, D. Joseph-McCarthy, L. Kuchnir, K. Kuczera, F.T.K. Lau, C. Mattos, S. Michnick, T. Ngo, D.T. Nguyen, B. Prodhom, W.E. Reiher, B. Roux, M. Schlenkrich, J.C. Smith, R. Stote, J. Straub, M. Watanabe, J. Wiorkiewicz-Kuczera, D. Yin, M. Karplus, All-atom empirical potential for molecular modeling and dynamics studies of proteins, J. Phys. Chem. B 102 (18) (1998) 3586–3616.

[49] W.L. Jorgensen, J. Chandrasekhar, J. Madura, P.W. Impey, M.L. Klein, Comparison of simple potential functions for simulating liquid water, J. Chem. Phys. 79 (1983) 926–935.

[50] E. Neria, S. Fischer, M. Karplus, Simulation of activation free energies in molecular systems, J. Chem. Phys. 105 (1996) 1902–1921.

[51] O. Galzitskaya, A. Caflisch, Solution conformation of phakellistatin 8 investigated by molecular dynamics simulations, J. Mol. Graphics Modell. 17 (1999) 19–27.

[52] C.L. Brooks Jr., M. Karplus, Solvent effects on protein motion and protein effects on solvent motion, J. Mol. Biol. 208 (1989) 159–181.

[53] J. Aqvist, Long-range electrostatic effects on peptide folding, FEBS Lett. 457 (1999) 414–418.

[54] D. Beglov, B. Roux, Finite representation of an infinite bulk system: solvent boundary potential for computer simulations, J. Chem. Phys. 100 (1994) 9050–9063.

[55] J.P. Ryckaert, G. Ciccotti, H.J.C. Berendsen, Numerical integration of the Cartesian equation of motion of a system with constraints: Molecular dynamics of *n*-alkanes, J. Comput. Phys. 23 (1977) 327–341.

[56] W. Kabsch, C. Sander, Dictionary of protein secondary structure: pattern recognition of hydrogen-bonded and geometrical features, Biopolymers 22 (1983) 2577–2637.

[57] H. Liu, S. Farr-Jones, N.B. Ulyanov, M. Llinas, S. Marqusee, D. Groth, F.E. Cohen, S.B. Prusiner, T.L. James, Solution structure of Syrian hamster prion protein rPrP (90–231), Biochemistry 38 (1999) 5362–5377.

[58] J.K. Myers, T.G. Oas, Contribution of a buried hydrogen bond to lambda repressor folding kinetics, Biochemistry 38 (1999) 6761–6768.

[59] M.E. Milla, B.M. Brown, C.D. Waldburger, R.T. Sauer, P22 arc repressor: transition state properties inferred from mutational effects on the rates of protein unfolding and refolding, Biochemistry 34 (1995) 13914–13919.

[60] R.B. Petersen, P. Parchi, S.L. Richardson, C.B. Urig, P. Gambetti, Effect of the D178N mutation and the codon 129 polymorphism on the metabolism of the prion protein, J. Biol. Chem. 271 (1996) 12661–12668.

[61] I. Bahar, A. Wallqvist, D.G. Covell, R.L. Jernigan, Correlation between native-state hydrogen exchange and cooperative residue fluctuations from a simple model, Biochemistry 37 (1998) 1067–1075.

[62] S.E. Radford, M. Buck, K.D. Topping, C.M. Dobson, P.A. Evans, Hydrogen exchange in native and denatured states of hen egg-white lysozyme, Proteins: Struct. Funct. Genet. 14 (1992) 237–248.

[63] J. Clarke, A.M. Hounslow, M. Bycroft, A.R. Fersht, Local breathing and global unfolding in hydrogen exchange of barnase and its relationship to protein folding pathways, Proc. Natl. Acad. Sci. U.S.A. 90 (1993) 9837–9841.

[64] A.E. Garcia, G. Hummer, Conformational dynamics of cytochrome C: correlation to hydrogen exchange, Proteins: Struct. Funct. Genet. 36 (1999) 175–191.

[65] M.P. Morrissey, E.I. Shakhnovich, Evidence for the role of PrP(C) helix 1 in the hydrophilic seeding of prion aggregates, Proc. Natl. Acad. Sci. U.S.A. 96 (1999) 11293–11298.

[66] D.R. Booth, M. Sunde, V. Bellotti, C.V. Robinson, W.L. Hutchinson, P.E. Fraser, P.N. Hawkins, C.M. Dobson, S.E. Radford, C.C. Blake, M.B. Pepys, Instability, unfolding and aggregation of human lysozyme variants underlying amyloid fibrillogenesis, Nature 385 (1997) 787–793.

[67] L. Calzolai, D.A. Lysek, P. Guntert, C. von Schroetter, R. Riek, R. Zahn, K. Wüthrich, NMR structures of three single-residue variants of the human prion protein, Proc. Natl. Acad. Sci. U.S.A. 97 (2000) 8340–8345.

[68] P. Kraulis, MOLSCRIPT: a program to produce both detailed and schematic plots of protein structures, J. Appl. Crystallogr. 24 (1991) 946–950.

[69] R. Koradi, M. Billeter, K. Wüthrich, MOLMOL: a program for display and analysis of macromolecular structures, J. Mol. Graphics Modell. 14 (1996) 51–55.